

RAPID FORMATION OF BLACK HOLES IN GALAXIES: A SELF-LIMITING GROWTH MECHANISM

ZHI LI^{1,2,5}, J. A. SELLWOOD^{3,4,6} AND JUNTAI SHEN^{1,2,7}

¹Key Laboratory for Research in Galaxies and Cosmology, Shanghai Astronomical Observatory, Chinese Academy of Sciences, 80 Nandan Road, Shanghai 200030, China

²University of China Academy of Sciences, 19A Yuquan Road, Beijing 100049, China

³Department of Physics and Astronomy, Rutgers University, 136 Frelinghuysen Road, Piscataway, NJ 08854

⁴Current address: Steward Observatory, University of Arizona, 933 N Cherry Ave, Tucson AZ 85721

Emails: ⁵lizh@shao.ac.cn ⁶sellwood@physics.rutgers.edu ⁷jshen@shao.ac.cn

Accepted to appear in the Astrophysical Journal

ABSTRACT

We present high-quality fluid dynamical simulations of isothermal gas flows in a rotating barred potential. We show that a large quantity of gas is driven right into the nucleus of a model galaxy when the potential lacks a central mass concentration, but the inflow stalls at a nuclear ring in comparison simulations that include a central massive object. The radius of the nuclear gas ring increases linearly with the mass of the central object. We argue that bars drive gas right into the nucleus in the early stages of disk galaxy formation, where a nuclear star cluster and perhaps a massive black hole could be created. The process is self-limiting, however, because inflow stalls at a nuclear ring once the mass of gas and stars in the nucleus exceeds $\sim 1\%$ of the disk mass, which shuts off rapid growth of the black hole. We briefly discuss the relevance of these results to the seeding of massive black holes in galaxies, the merger model for quasar evolution, and the existence of massive black holes in disk galaxies that lack a significant classical bulge.

Keywords: galaxies: ISM — galaxies: kinematics and dynamics — galaxies: structures — galaxies: hydrodynamics — galaxies: formation — quasars: supermassive black holes

1. INTRODUCTION

Most galaxies host massive black holes in their centers (Kormendy & Richstone 1995), although many are dormant. Black holes are believed to power quasars, which are thought to have short lifetimes in the bright phase (Martini 2004). It is well established that the co-moving space density of quasars peaks at intermediate redshift (e.g. Boyle et al. 1987; Hopkins et al. 2007b; Singal et al. 2016). The rise of this activity from the time of the early universe to $z \sim 3$ coincides with galaxy assembly that is driven by gravitational instability, when gas is abundant (see Somerville & Davé 2015, for a recent review). The usual idea is that most quasar activity is caused by galaxy mergers, which drive gas into the nucleus (Toomre & Toomre 1972; Hopkins et al. 2007a; Treister et al. 2012; Bonoli et al. 2014). The decline in the quasar luminosity function since $z \sim 2$ is attributed to a variety of factors (Merloni & Heinz 2008): the decrease in the galaxy merger rate as the universe expands, a decrease in the gas content of galaxies (e.g. Morokuma-Matsui & Baba 2015), and feedback (Wyithe & Loeb 2003; Di Matteo et al. 2005), although exactly how feedback extinguishes activity is difficult to model (e.g. Hopkins et al. 2005; Dubois et al. 2012).

However, the merger model for quasar activity implicitly pre-supposes the pre-existence of moderate mass black holes in the merging galaxies. Furthermore, stars formed prior to a galaxy merger are expected to accumulate into a classical bulge (but see Keselman & Nusser 2012, for a dissenting view), which is absent in some significant fraction of galaxies (Kormendy et al. 2010). None of the galaxies lacking classical bulges listed by Kormendy et al. (2010) have measured black hole masses but some have an AGN that is a clear indicator of a

moderately massive black hole, hereafter MBH.¹ Two specific examples are (a) NGC 5746, which has no classical bulge (Barentine & Kormendy 2012) but has an X-ray bright Seyfert nucleus (González-Martín et al. 2009), and (b) the dwarf galaxy RGG 118 that has a pseudobulge and an AGN, for which Baldassare et al. (2017) estimate a BH mass of $\sim 5 \times 10^4 M_{\odot}$. A path must therefore exist to form a MBH in a galaxy that does not involve mergers.

The formation of seed BHs has received a lot of attention (see Latif & Ferrara 2016; Smith et al. 2017, for recent reviews), but a convincing model remains elusive. Some have argued (e.g. Madau & Rees 2001) that the seeds are stellar mass BHs in the early universe. A second idea is runaway collapse of star clusters (e.g. Shapiro & Teukolsky 1985; Ebisuzaki et al. 2001). The third suggestion, which continues to be intensively studied, is the direct collapse of a gas cloud to form a BH with a seed mass of $\sim 10^4$ – $10^7 M_{\odot}$ (e.g. Haehnelt & Rees 1993; Luo et al. 2016).

Sellwood & Moore (1999, hereafter SM99) presented a little known alternative scenario. They suggested that MBHs could be created at the centers of forming galaxies, where gas is concentrated into a small volume through the action of a rotating bar. We here review the ingredients of their model, which attempts to account both for the creation of MBHs and their subsequent quiescence. Similar ideas were also advanced independently in a much later paper by Fanali et al. (2015).

The model proposed by SM99 relates to the period of disk galaxy assembly. It starts from the well-known finding (Ostriker & Peebles 1973; Toomre 1981;

¹ We use MBH to indicate BHs with masses over a broad range up to $\sim 10^7 M_{\odot}$.

Berrier & Sellwood 2016) that the formation of a largely rotationally supported galactic disk would naturally lead to the early formation of a bar. SM99 argued that the initial absence of a central mass concentration would allow gas to be driven inward as far as the bar torque could achieve. They then speculated that a fraction of the gas that accumulates in the center may collapse to grow and power a MBH, while the remainder contributes to a central mass concentration of stars and gas.² They concluded that inflow driven by the early bar would have built up a sufficiently massive central object that the later gas inflow would stall at distances of a few hundred parsec from the nucleus. In their picture, the early formation of a bar grows the MBH, but the associated nuclear activity subsides soon thereafter because the build up of the central mass causes the inflow to stall at a nuclear ring, thereby halting the rapid growth of the MBH.

Although the formation of a MBH from the gas concentration remains purely speculative, the remainder of the overall picture rests on many well-established aspects of galaxy dynamics. It has long been known (e.g. Gerin et al. 1988; Sakamoto et al. 1999) that bars drive large amounts of gas into galaxy centers, and Fanali et al. (2015) emphasized that substantial inflow occurs during the process of bar formation. Work by others, (e.g. Athanassoula 1992; Kim et al. 2012b), has indicated that the inflow often stalls at a gaseous ring having a radius a few hundred parsec, which plausibly corresponds to observed star-forming nuclear rings (Buta 1995). Circum-nuclear star-forming gaseous rings are preferentially found in barred galaxies, leading to a correlation between bars and enhanced central star formation (e.g. Hawarden et al. 1986; Jogee et al. 2005; Mazuca et al. 2008; Hao et al. 2009; Lin et al. 2016).

However, nuclear rings are not always formed in bar-driven flows, and can be absent in cases where the central potential well of the galaxy is relatively shallow, i.e. when the galaxy lacks a central massive object. We explain this dichotomy of behavior in section 3.

A strength of the model proposed by SM99 is that the process of forming the MBH is self-limiting. The build up of the central massive object eventually causes gas inflow down the bar to stall at a nuclear ring. While some have argued (e.g. Wada 2004) for mild, spiral-driven inflow within the ring, it must be at a much slower rate, else the ring would not feature a gas density excess. Furthermore, accretion onto the MBH would require the gas from the ring to be carried inwards to $\lesssim 1\%$ of the ring radius. Thus the fuel supply to the AGN is choked off by the formation of the nuclear ring and MBH activity will decline.

SM99 included a growing massive central object in their models and found, as is widely known (Norman et al. 1996; Shen & Sellwood 2004), that the bar may be weakened or even be dissolved as its mass was increased. Kormendy & Kennicutt (2004) argue that these secular internal processes of bar-driven inflow causing the eventual dissolution of the bar lead to the formation of “pseudobulges”, which are thickened central components with disk-like density profiles and velocity distributions that may be formed without early galaxy

mergers.

SM99, and also Bournaud & Combes (2002), showed that on-going accretion onto the disk of a galaxy may allow a second bar to form later, but the massive compact object created in the first bar-forming episode will cause gas inflow to stall at a nuclear ring, preventing the MBH from becoming active again.

The purpose of the present paper is to determine the critical mass of the central compact object needed to cause the bar-driven inflow to stall at a nuclear ring, an issue that SM99 could not address since their simulations lacked a gas component. We use 2D hydro simulations in realistic barred potentials to determine the central mass needed to arrest the inflow at a nuclear ring. We also estimate the likely masses of the MBHs that could be formed before the nuclear ring is established.

2. MODEL SETUP

2.1. Hydrodynamical Simulation

We simulate gas flow in a rigid, rotating, non-axisymmetric barred galaxy potential, focusing on the effects of massive central objects on bar-induced inflow. As the setup and the numerical methods used in our simulations are very similar to those in Li et al. (2015), we give only a brief summary here. We solve Euler’s equations of ideal hydrodynamics in the bar corotating frame using the grid-based MHD code *Athena* (Gardiner & Stone 2005; Stone et al. 2008; Stone & Gardiner 2009). The gaseous disk is stirred by an external barred potential, described in Section 2.2, that is assumed to rotate rigidly about the galactic center with a fixed pattern speed $\Omega_{\mathbf{b}} = \Omega_b \hat{\mathbf{z}}$. We adopt a 2D isothermal, rotating gaseous disk with an initially uniform surface density of $\Sigma_0 = 15 M_{\odot} \text{pc}^{-2}$, and neglect magnetic fields, and other additional physics, except that we include self-gravity in one case.

We employ a uniform Cartesian grid with 4096×4096 cells covering a box of size of $L = 12.6$ kpc in each direction. Thus the grid spacing is $\Delta x = \Delta y = 3.1$ pc. We adopt the *exact* nonlinear Riemann solver and outflow boundary conditions at the domain boundaries for our hydrodynamic models. The importance of high spatial resolution and the exact Riemann solver has already been demonstrated in previous work (e.g. Sormani et al. 2015; Li et al. 2015; Few et al. 2016). We choose an effective isothermal sound speed of $c_s = 10 \text{ km s}^{-1}$ to describe the mean velocity dispersion in molecular clouds, similar to earlier studies (e.g. Fux 1999; Rodriguez-Fernandez & Combes 2008; Kim et al. 2012a). All the models are run for a period of 1 Gyr.

In one case only, we use Fourier transforms with periodic boundary conditions to compute the gravitational potential of the gas as it evolves. This self-gravity term is added to that of the externally applied bar potential.

2.2. Gravitational Potential

Previous simulations of gas flow in barred potentials have generally modeled the bar in one of two ways: as a rigid prolate spheroid (e.g. Athanassoula 1992; Kim et al. 2012b) or by using the potential from an N -body simulation in which a bar has formed through a disk instability (e.g. Fux 1997; Shen et al. 2010). It is easy to vary the parameters of a prolate spheroid, especially one with an

² Hereafter, we refer to the combined mass of gas, stars, and the MBH that reside in the center as a “massive central object.”

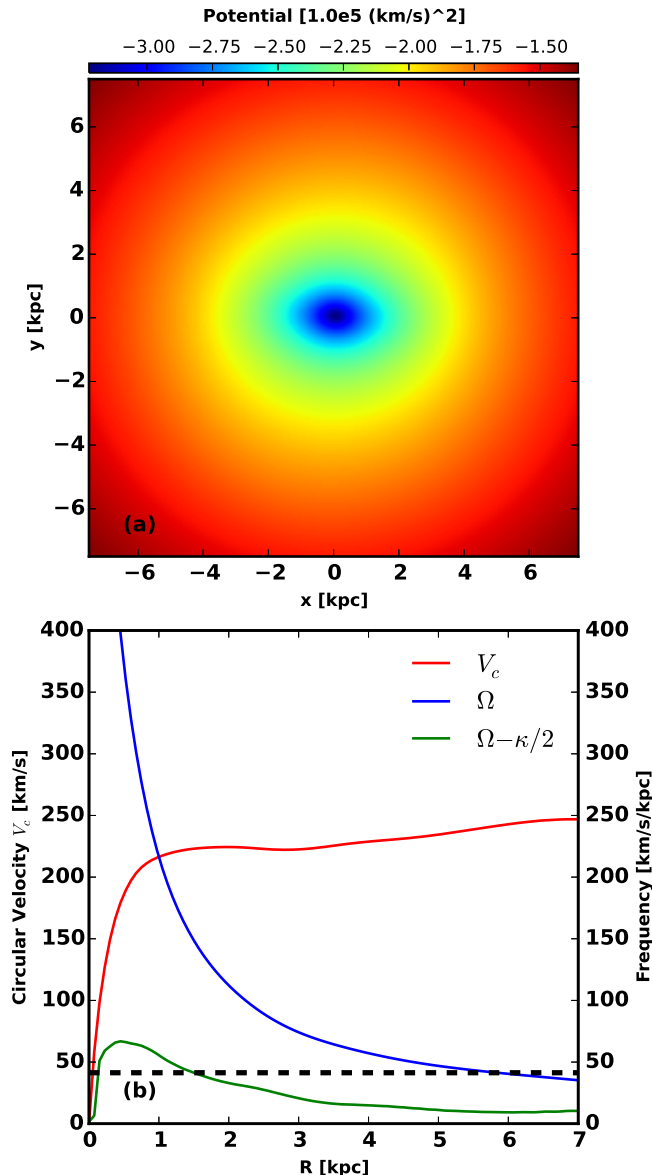


Figure 1. Upper panel: contours of the potential of the stacked N -body model in a stationary frame. The bar has a semi-major axis of ~ 3.5 kpc and is aligned with the x -axis. Bottom panel: the rotation curve of the model together with curves showing the principal angular frequencies, that were determined from the azimuthally averaged central attraction. The red line denotes the circular speed V_c , the blue line denotes $\Omega = V_c/R$, and the green line denotes $\Omega - \kappa/2$, where $\kappa^2 \equiv R^{-3}d(R^4\Omega^2)/dR$ (Binney & Tremaine 2008). The horizontal black dashed line shows the bar pattern speed, $\Omega_p = 41.35 \text{ km s}^{-1} \text{ kpc}^{-1}$ and the co-rotation resonance is at $R \sim 5.7$ kpc.

analytic potential, but an N -body bar is both dynamically self-consistent and is generally a better match to observed bars, as we show in Section 4. Here we prefer to use the potential from an N -body simulation.

2.2.1. N -body Potential

We use the mid-plane potential from an N -body model created using the *GALAXY* code (Sellwood 2014). It is the model shown in Figures 6.18 and 6.35 of Binney & Tremaine (2008). The model began with an exponential disk that was thickened with a $\text{sech}^2(z/2z_0)$

vertical density profile. The disk was embedded in a live halo that was compressed (Sellwood & McGaugh 2005) by the addition of the disk from the initial density distribution with an isotropic distribution function given by Hernquist (1990). The uncompressed halo had a nominal mass 80 times and a scale radius 30 times those of the disk, but any halo particles that would pass beyond a radius of $60R_d$ were discarded, reducing the halo mass to just over 20 times the disk mass. The disk was represented by 1 million particles and the halo by 2.5 million. The mass of the disk was $3.0 \times 10^{10} M_\odot$ and its length scale was 1.5 kpc.

We extracted the mass distribution of the simulated barred model at 26 moments over the period 225 to 250 dynamical times, where the dynamical time is 5 Myr. As illustrated in Fig 6.35 of Binney & Tremaine (2008), this period is well after the bar had formed, buckled, and settled. We stacked the separate mass distributions after rotating each to a common bar major axis, assuming a steady rotation rate at the best-fit pattern speed over this interval, and derived the in-plane forces and potential from this time-averaged mass distribution.

The top panel of Figure 1 shows the potential, in an inertial frame, in the mid-plane of this mass model. The bar has a mean pattern speed of $\Omega_b = 41.35 \text{ km s}^{-1} \text{ kpc}^{-1}$ and bar strength parameter $Q_b = 0.40$ that implies a strong bar.³ The lower panel of this Figure shows the corresponding rotation curve and usual angular frequencies that were derived from the azimuthally averaged central attraction. The corotation radius is therefore at $R_c \simeq 5.7$ kpc and $\mathcal{R} \equiv R_c/a_B \simeq 1.6$, where the semi-major axis of the bar, $a_B \simeq 3.5$ kpc, was estimated by the method described in Debattista & Sellwood (2000).

As usual, the hydrodynamical simulations start from a circular flow pattern in the azimuthally averaged potential, and we compute the gas flow in a frame that corotates with the bar. To avoid subjecting the gas flow to a sudden change, we gradually diminish the axisymmetric potential to zero and substitute an increasing fraction of the bisymmetric one over the first 100 Myr.

2.2.2. Massive central objects

We find that a large amount of gas is quickly driven into a small volume at the center of the model. Since our simulations neglect many physical processes, they cannot predict the fate of this gas. However, SM99 argued that the principal dynamical consequence of the accumulated gas would be to create a massive central object, which may be composed of stars, gas, and a central MBH. The precise nature of the object is unimportant for the dynamics of the gas outside its small radial extent. In our models without gas self-gravity, we therefore model the consequence of the inflow by adding a central mass. We also present one case where self-gravity is included to show that the effect of mass accumulation in the center is well-captured by the addition of a massive compact object.

We have employed three different density profiles

³ Q_b is defined as the maximum ratio of the tangential force (mainly due to the non-axisymmetric bar potential) to the azimuthally-averaged radial force in the potential (e.g. Combes & Sanders 1981; Comerón et al. 2010).

(Plummer sphere, Hernquist, and modified Hubble) to model the massive central object:

$$\begin{aligned}\rho(r) &= \left(\frac{3M_{\text{Plum}}}{4\pi a^3} \right) \left(1 + \frac{r^2}{a^2} \right)^{-5/2}, \\ \rho(r) &= \left(\frac{M_{\text{Hern}} a}{2\pi r} \right) \frac{1}{(r+a)^3}, \\ \rho(r) &= \rho_{\text{Hubb}} \left(1 + \frac{r^2}{a^2} \right)^{-3/2}.\end{aligned}\quad (1)$$

Here M_{Plum} and M_{Hern} denote the total mass of the central object by the corresponding density profile, while ρ_{Hubb} represents the object central density for modified Hubble profile, and a is the scale length of the central objects. We compute the gas flow patterns when this component is added to the gravitational field of the N -body model, and compare the results with cases where it is omitted.

3. TWO DIFFERENT GAS FLOW PATTERNS

Here we report simulations of the gas evolution in the potentials described in Section 2.2. Since gas flows at highly supersonic speeds relative to the potential everywhere except close to the corotation resonance, strong shocks develop that are indicated by the high density gas ridges (Figure 2a). Those within the bar form on the leading side of the bar, as are typically found in all other work, and gas flows rapidly towards the center. This happens because gas loses both energy, due to the shocks, and (on average) angular momentum, since it is asymmetrically distributed with respect to the major-axis of the potential.

3.1. No central mass concentration

The nature of the inner gas flow is strongly dependent on the existence of an inner Lindblad resonance (ILR). In the absence of pressure forces, gas flows will settle onto stream lines that follow nearly circular periodic orbits. For a weak perturbing potential, linear theory (Sanders & Huntley 1976; Binney & Tremaine 2008) predicts that the orientation of a near circular closed loop orbit switches from parallel to the bar on the side nearer to corotation to perpendicular to the bar inside the ILR.

Note that the condition $\Omega_b = \Omega - \kappa/2$ determines the existence and locations of Lindblad resonances only for a bar of infinitesimal amplitude. Not only do the circular and epicycle frequencies require generalization to action-angle variables in a bar of finite amplitude, but the existence of resonances can be determined only from orbit integrations – see Contopoulos & Grosbol (1989), Sellwood & Wilkinson (1993) or Binney & Tremaine (2008) for reviews. Many families of orbits have been identified in steadily rotating bar-like potentials, even when motion is confined to a plane, but only two are of importance here. The main family of bar-supporting orbits, known as x_1 , is aligned parallel to the bar when viewed from a frame that rotates with the bar. However, a second family, known as x_2 , that is aligned perpendicularly to the bar often exists deep inside the bar. The change of orientation suggests that Lindblad’s concept of a resonance can be generalized to non-linear perturbations (van Albada & Sanders 1982; Li et al. 2015), and

we hereafter extend the acronym ILR to indicate the existence of the x_2 orbit family in perturbations of finite amplitude.

Since the flow must have a unique velocity everywhere, pressure and possibly shocks change the flow pattern where orbits intersect – for example in the region where orbit orientations switch from parallel to perpendicular. If this were to happen, we usually find that the inflow stalls, and a dense, moderately eccentric, ring of gas builds up where the x_2 orbits are found.

A necessary, but not sufficient, condition for the presence of the x_2 family is that a weak bar of a given pattern speed should possess two ILRs in the azimuthally averaged potential, as in the case in our model, as shown in Figure 1(b). However, it has long been known (Contopoulos & Papayannopoulos 1980) that the possible energy⁴ range of x_2 orbits narrows, and may vanish entirely, as the strength of the bar perturbation is increased.

Indeed, no x_2 orbits exist in the strongly barred potential of our original N -body model and therefore no ILRs were present in our first model lacking a central mass concentration. In this case, therefore, gas was driven as far inward as we could resolve, as was argued by SM99. In Figure 2(a) the high density gas ridges extend from $R \sim 2.5$ kpc to very close to the center, indicating that gas is driven into the nuclear region. Although, our idealized hydrodynamic simulations cannot predict the ultimate fate of the inflowing gas, it seems plausible that a high concentration of stars will be formed, while some of the gas may connect to an accretion disk to create a MBH.

The timescale for the inflow is also very short: during the first 100 Myr when the bar is being established, a large fraction of the gas has already been driven to the center. By $t = 300$ Myr, nearly all the gas inside bar corotation radius has been driven to a highly eccentric structure with corresponding streaming velocities. The flow pattern, which is shown at $t = 400$ Myr in Figure 2(b), then becomes quasi-steady until the end of the simulation mainly because we do not model the additional physical processes that would probably consume the high density gas around the center.

3.2. Including a central mass concentration

We wish to understand how the flow pattern is affected by the accumulation of mass in the center. In order to achieve this without including gas self-gravity, we ran a series of additional simulations in which we simply included the potential of central objects of differing masses, described by one of the equations (1), into that of the original N -body model. The massive central object was introduced at the beginning of each simulation and was not changed while the simulation runs.

Periodic orbit studies in these modified potentials confirm the existence of x_2 orbit family (i.e. an ILR) when we include a central object of at least $\sim 3 \times 10^8 M_\odot$, which is $\sim 1\%$ of that of the galactic disk. Although the bar is the same, an ILR is enabled by the higher frequencies of the inner orbits in the deeper potential well

⁴ More correctly, Jacobi constant, $E_J = E - \Omega_b L_z$ which is an energy-like conserved quantity in a rotating non-axisymmetric potential.

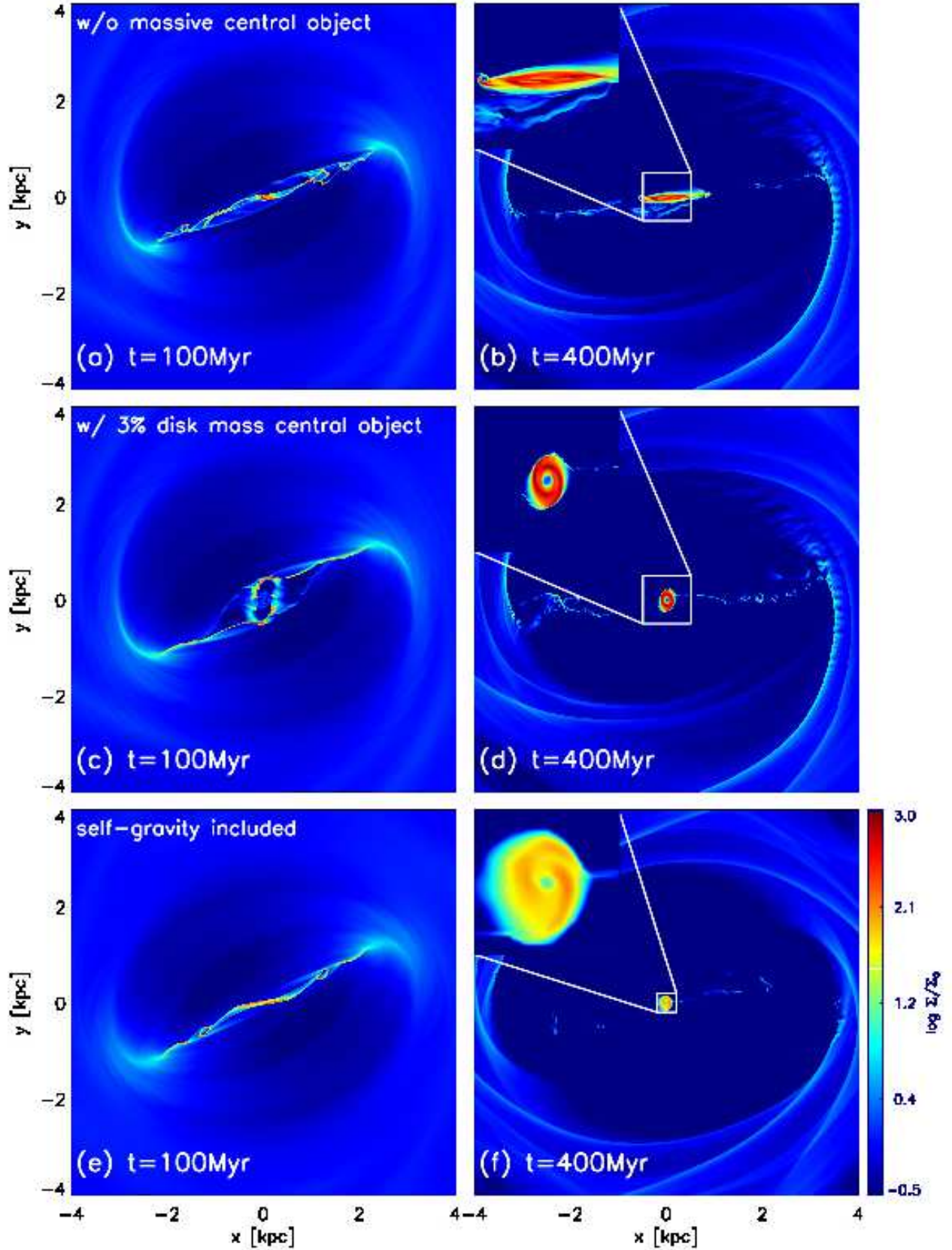


Figure 2. The evolution of the gas surface density in models both without and with a massive central object. The color scale is logarithmic. Panels (a) and (b) are for the N -body model potential at two times, (c) and (d) illustrate the flow when a massive central object is included, while (e) and (f) show the bar model with gas self-gravity and no central object. Note that the massive central object greatly alters the gas behavior in the central part ($R \lesssim 1$ kpc), while the outer flow patterns ($R \gtrsim 4$ kpc) are almost identical.

created by the central mass.

Figure 2(c) and (d) shows the gas flows at $t = 100$ Myr and $t = 400$ Myr respectively when the central object was a Plummer sphere with a scale length $a = 100$ pc and mass $M_{\text{Plum}} = 9.0 \times 10^8 M_{\odot}$, which is 3% of the disk mass. In contrast to the run where no ILR is present (panels a and b), the high density gas ridges curve around the center at their inner ends and do not approach closer than ~ 400 pc to the center, which is the approximate radius of the ILR, see §4.2. The later gas flow forms a ring-like structure with very little further inflow, which is similar to nuclear rings often observed in barred galaxies. Once an ILR is present, little, if any, of the bar-induced inflow can reach the nuclear region, and the activity of the MBH must decline as the immediately surrounding fuel is no longer being replenished by bar inflow.

3.3. Inclusion of gas self-gravity

In order to test whether an artificially added massive compact object adequately mimics the self-regulated process of mass inflow, we here present a simulation that includes gas self-gravity and no externally imposed massive central object.

However, the inclusion of self-gravity is not straightforward because an isothermal equation of state prevents the internal pressure from rising as gas contracts under its own self-gravity, causing a runaway density increase, as is well known. Thus, naively including the self-gravity term caused the central gas disk in our model to contract continuously with no more than a hint of a transient nuclear ring. Changing to an adiabatic equation of state was not a solution, since shocked gas remained hot, and the entire flow quickly ceased to be super-sonic, inhibiting almost all inflow of gas to the bar center. The isothermal assumption is physically more reasonable, as gas in galaxies dissipates energy efficiently, but dense gas also fragments to form stars, with energy feedback on small-scales that is challenging to model. The galaxy formation community adopts rules to try to capture the unresolvable “sub-grid physics” of star formation (e.g. Scannapieco et al. 2012). These rules are themselves no more than physically-motivated guesses and, for our purpose, are both too time consuming and complicated, since we do not need to track the highly local re-expansion and pollution of the gas, the ages and chemistry of the stars, etc.

We therefore adopted a simpler approach.

- We model a steady rate of star formation by continuously removing mass from the gas and replacing it with a growing rigid mass distribution to represent the gravitational attraction of the newly-formed stars. Starting at $t = 150$ Myr, when some gas had already accumulated in the center, we removed a fraction of gas having a 2D exponential density profile from the gaseous disk at every time step, while adding the gravitational attraction of the removed gas to the rigid background potential. We chose a scalelength of 10 pc for the exponential profile, and froze 1% of the surface density at center at each time step. Our results were insensitive to reasonable variations of these parameters, but a much lower freezing fraction caused too slow a rise in the mass in stars.

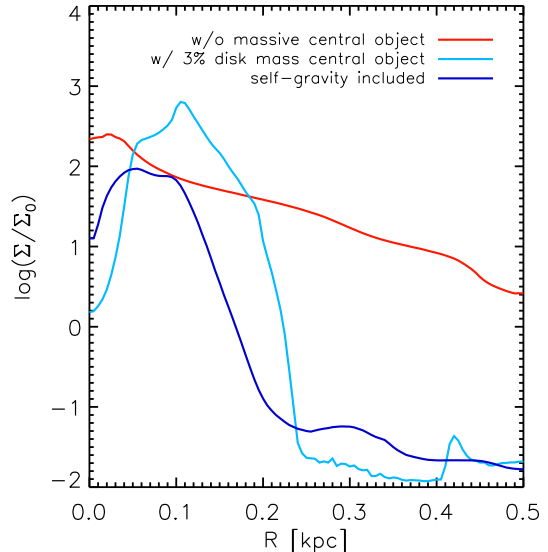


Figure 3. The gas density profile along the bar minor axis at $t = 400$ Myr in the three simulations shown in Figure 2. The red curve is for the run with no central object, the cyan curve is for the run with a rigid central object, and the blue curve is for the run with self-gravity.

- We found that the nuclear gas disk was destabilized by a minor asymmetry in our N -body model, which created a rotating, mildly lop-sided component to the rigid forcing potential. We therefore imposed 4-fold symmetry by reflecting the potential about the x - and y -axes and averaging.
- We increased the initial gas surface density to $30 M_{\odot} \text{pc}^{-2}$, resulting in a gas fraction that is $\sim 10\%$ of the stellar disk mass inside the bar co-rotation radius. Though large for present-day galaxy disks, such a gas fraction is probably on the low side for galaxies in the early universe.

The flow pattern in this case is shown in panels (e) and (f) of Figure 2. The evolution for the first 100 Myr resembles that shown in (a), but panel (f) shows a ring-like structure by $t = 400$ Myr in a manner that more closely resembles that shown in panel (d), and the ring persists until the end of the simulation (1 Gyr). In this case, the mass of frozen gas is $7.1 \times 10^8 M_{\odot}$ at $t = 400$ Myr, rising slightly to $7.8 \times 10^8 M_{\odot}$ by $t = 1$ Gyr, which is approximately 2.6% of the disk mass. Note that the rate of star formation in this bar-driven nuclear starburst is less than $3 M_{\odot} \text{yr}^{-1}$, when averaged over the interval 150 – 400 Myr, in line with present-day estimates for barred galaxies (e.g. Davies et al. 2017). Thus the mass of gas that reaches the central parts in this model is comparable to that we assumed for the rigid mass concentration in the middle row of Figure 2, and is sufficient to cause an ILR that stalls the inflow, as discussed above.

Figure 3 shows the azimuthally averaged gas density profile in all three simulations shown in Figure 2. The red curve is for the run with no central object for which the density rises all the way to the center. The cyan curve shows the ring-like feature that formed in the run with a rigid central object. The blue curve is for the run

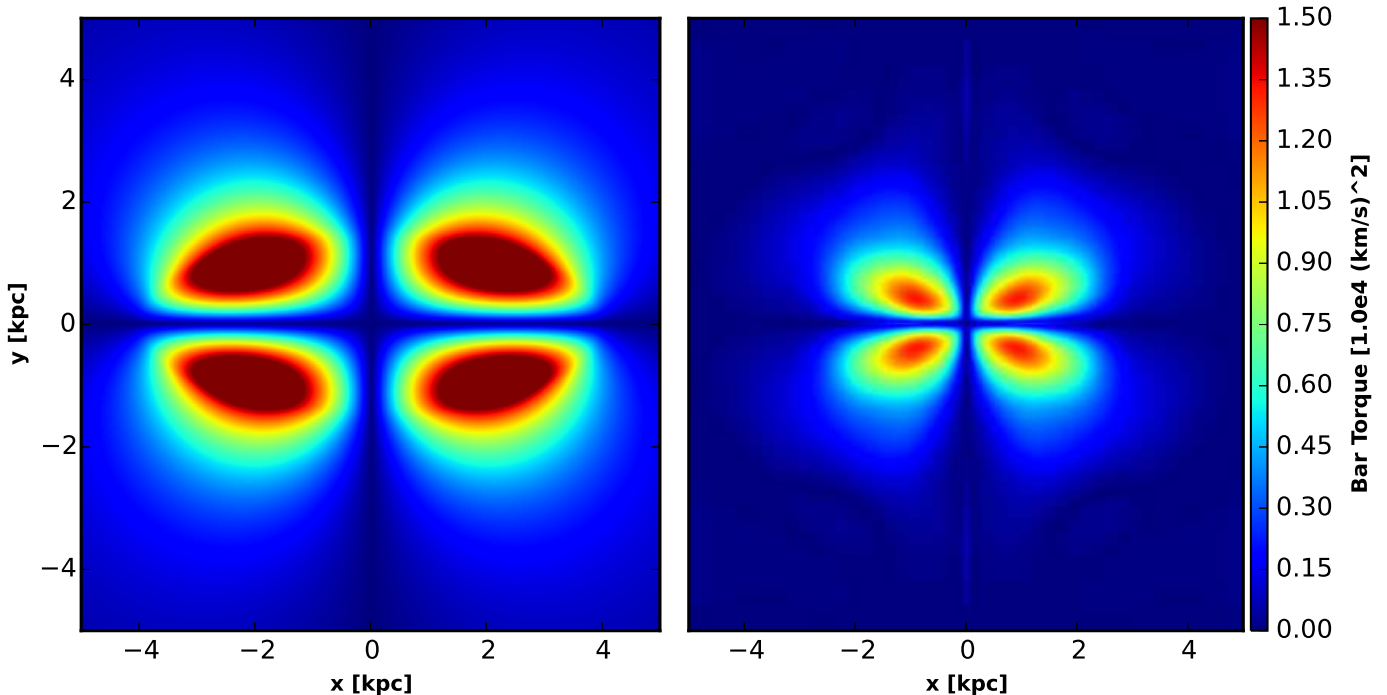


Figure 4. The bisymmetric torque $|\mathbf{R} \times \mathbf{F}|$ for an $n = 1$ Ferrers prolate spheroid (left panel) and for the N -body bar we used (right panel). The spheroid has semi-major and semi-minor axes of 4.0 kpc and 1.5 kpc, similar to the shape of the N -body bar, and the bar strength parameter $Q_b = 0.40$ for both bars.

with self-gravity, which also presents a ring-like structure. These results clearly show that, when self-gravity is included, the bar-driven flow creates a central mass concentration that, once established, causes the subsequent inflow to stall at ~ 100 pc from the center.

4. TESTS

The large-scale gas flows presented in the previous section support the evolution scenario proposed in SM99. They suggest that bars may contribute to AGN activity for only a very short time due to the rapid response of gas to the barred potential. Most inflow may occur during the bar formation episode, as reported by Fanali et al. (2015), and nuclear activity should cease soon after the bar and the ILR are fully established.

In this section, we present tests to demonstrate that our results are affected neither by the barred model nor by the density profile of the massive central object we adopt. However, we do find some evidence for mild numerical diffusion at $R \lesssim 100$ pc.

4.1. Bar model

The gas flow patterns are sensitive to the adopted potential of the bar because its shape and mass determine the torque, $|\mathbf{R} \times \mathbf{F}|$, acting on the gas; here \mathbf{R} and \mathbf{F} are the position and gravitational force vectors, respectively. Figure 4 compares the distributions of the bar torque for our N -body bar with that of a similar size $n = 1$ Ferrers prolate spheroid that has a similar axis ratio $b : a = 3 : 8$, and almost the same Q_b parameter. We see that the forces from the N -body bar differ significantly from those of the spheroid model in the sense that the high torque regions in the N -body bar form more of an X-shape and are more centrally concentrated. Not only is this very

similar to the corresponding maps derived from the photometry of barred galaxies (Buta & Block 2001), but the stronger torques at small radii can drive gas closer to the center.

We find that the gas flow patterns in the N -body bar differ slightly from those in the Ferrers potential, which we adopted in our previous work (Li et al. 2015). A gaseous “inner ring” that lies on the edge of the bar is commonly seen in the simulations using a prolate spheroid (e.g. Athanassoula 1992; Kim et al. 2012a), while such a feature has not been found in observations⁵. In addition, Fragkoudi et al. (2016) argued that boxy/peanut (B/P) bulges reduce the amount of gas reaching the central regions. The formation of B/P bulges is a natural consequence of an N -body bar, while a prolate spheroid is not a close match to a B/P shape. We therefore conclude that gas flow patterns in an N -body bar may better match those in galaxies.

Since our bar model is somewhat “slow” ($\mathcal{R} \sim 1.6$) we also tested the “fast” bar from Shen et al. (2010), for which $\mathcal{R} \simeq 1.2$. We found that the gas flow patterns are almost identical to those presented in §3, suggesting that the critical central mass of 1% disk mass is a robust result for different N -body bars.

4.2. Different central masses

We found (§3) that x_2 orbits (or an ILR) that cause the gas inflow to stall in a nuclear ring are present only in models that include a massive central object. Here we study the extent to which the choice of parameters of the

⁵ It is worth noting that the power-law density prolate spheroid bar model used in Binney et al. (1991) is more similar to an N -body bar both in the torque distribution and in the resulting gas flow pattern.

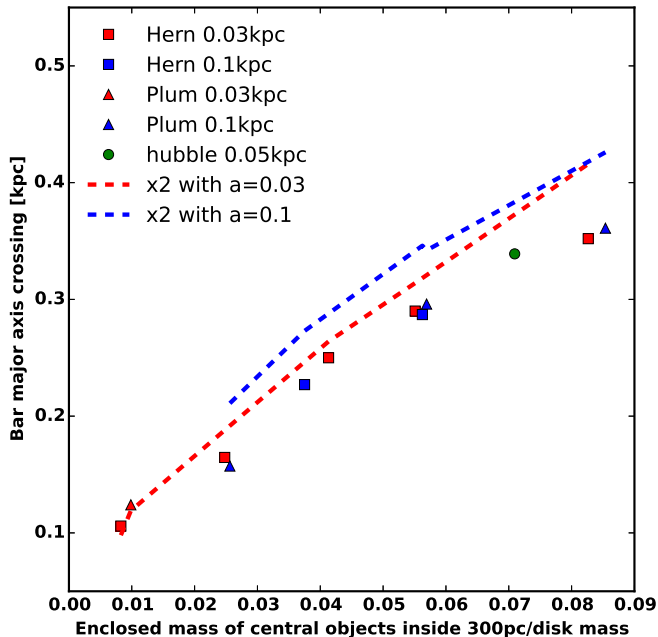


Figure 5. The ring outer radius at $t = 400$ Myr as a function of the mass of the central object enclosed mass inside 300 pc, expressed as a fraction of the disk mass. The squares are from the simulations using Hernquist profile and the triangles are using Plummer sphere. Red and blue represent the models having a scale length of 0.03 kpc and 0.1 kpc. The green circle is from a simulation using modified Hubble profile with a scale length of 0.05 kpc and an enclosed mass of $2.0 \times 10^9 M_{\odot}$ at $R = 300$ pc. The dashed lines show the major axis crossing of the largest non-intersecting x_2 orbits for two different values of the bulge scale parameter a .

massive central object affects the inner part of the flow pattern. We compare results from two density models: a Hernquist profile with a scale length of 30 pc to represent a cusped central object, and a Plummer sphere with a scale length of 100 pc to represent an object with an harmonic core, and vary the mass for each over the range 1% to 10% of the disk mass. In each case we estimated both the outer radius of, and mass of gas in, the nuclear ring.

In the absence of thermal pressure or other forces acting on the gas, the stream lines will follow periodic orbits that do not intersect. However, shocks will remove gas from orbits that do intersect. The highest energy x_2 orbits are skinnier than those of lower energy and intersect with some of them. Thus, the gas must settle onto the lower energy x_2 orbits that are smaller and rounder than those of the highest energy. We therefore expect the nuclear ring to form approximately near the inner edge of the range of x_2 orbits, although the correspondence may not be exact since pressure forces may also affect the motion of the gas to a small extent.

The variation of the ring radius as a function of the mass of the central object enclosed within 300 pc is plotted in Figure 5. We find that a more massive central object with a smaller scale length results in a larger ring outer radius. We conclude that the radius where the flow stalls depends most strongly on the mass of the central object and is less sensitive either to the density profile or to its scale length over the tested range. The dashed lines plot the central distance at which the largest x_2 orbit that does not intersect other x_2 orbits crosses the

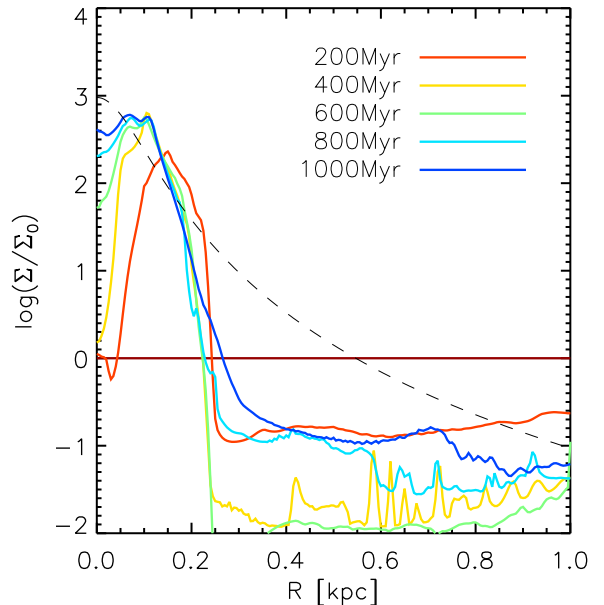


Figure 6. Normalized azimuthally averaged gas surface density inside 1 kpc in the simulation using a Plummer sphere with a mass of $9.0 \times 10^8 M_{\odot}$ and a scale length of 0.1 kpc. The colors represent gas density at different time. The initial density distribution is shown by the horizontal deep red line. The ring becomes a disk at around 600 Myr. We also draw the surface density of a Plummer sphere with a scale radius of 0.1 kpc and a mass of $4.5 \times 10^8 M_{\odot}$ using the black dashed line.

bar major axis for two different values of the bulge scale parameter. It is clear from this Figure that rings form where gas can settle onto non-intersecting x_2 orbits.

We also find that the total mass of the ring is about the same ($\sim 4.5 \times 10^8 M_{\odot} \sim 1.5\%$ disk mass) in all the models, regardless of the masses or scale sizes of the central object. Probably this is simply a consequence of holding the bar size, pattern speed, etc., as well as the gas density, fixed in all our simulations. See Li et al. (2015) for more discussion.

Note that the lowest central density Plummer model, with 1% of the disk mass and 100 pc scale length, did not form a nuclear ring (i.e. gas flowed to the very center), but a ring did form at the same mass when we reduced its length scale to 30 pc. Considering the intrinsic scatter in observed bar properties and the fact that nuclear star clusters are very dense, we conclude a massive central object with about $\sim 1\%$ disk mass is enough to prevent further inflow to the MBH.

4.3. The inner boundary of the ring

The gaseous nuclear ring formed due to the massive central object usually presents an inner boundary, and we find little gas inside. However, we observe that the inner boundary shrinks with time and eventually the ring may fill to become a disk (Figure 6). Since we wish to be clear whether the processes we include in our simulations do or do not allow gas to reach the center and accrete onto a MBH, we have tested whether the filling of the ring is physical or numerical.

We performed simple simulations that began with a rotating isothermal gaseous ring, having a sharp inner

boundary, in the axisymmetric potential of an exponential disk. We varied the spatial resolution and the sound speed and studied whether the boundary blurred over time. We found that simulations with at least 30 grid points inside the inner boundary maintained a sharp edge, while with fewer than 20 grid points inside the initial edge the ring gradually diffused inwards, filling the hole completely after a few tens of orbit periods. Thermal effects on spreading the boundary were negligible as long as the rotation velocity was large compared with the sound speed.

We have also used the static mesh refinement (SMR) technique to better resolve the central regions of the simulations using the bar model, finding that the ring lasts for a longer time before filling in the SMR runs. We therefore conclude that the spreading of the inner boundary in our simulations is caused by numerical diffusion, and that simple hydrodynamics alone would predict that an ILR would perfectly cut off the supply of gas to a MBH in the galactic center. Note it is possible that other physical processes could intervene to bring gas from the nuclear ring to the MBH as we discuss below.

5. DISCUSSION

5.1. *Mass of the central BH*

In order to form a MBH, the angular momentum of gas in the disk of a galaxy must be reduced by many orders of magnitude. Accretion disks and dusty tori are invoked for the last stages (e.g. Krolik 1999), but gas must be brought to a radius of a few parsec before they can take over. We have found, in common with most other work, that a large fraction of the gas in the bar region is driven very close to the center in the first ~ 100 Myr. We also found from our run with self-gravity, Figure 2(f), that inflow is stalled at a well-established nuclear ring ~ 400 Myr after the start. Thus abundant gas is present in the nuclear region for some ~ 300 Myr.

Here we make no attempt to calculate the evolution of this gas concentration, and confine ourselves to speculation. A MBH may form through a cascade of instabilities to ever smaller scales, along the lines of the models proposed by Shlosman et al. (1989) and Hopkins & Quataert (2010), but without the pre-existing MBH. Alternatively, vigorous star formation in such environment could lead to the runaway growth of a massive star (Krumholz 2015).

Whatever the initial mass of the BH, the rich reservoir of gas in the nucleus will enable it to grow rapidly. In order to make a very rough estimate of the mass of the MBH that may be formed, we assume that the proto-BH accretes $\sim 0.01 M_{\odot}$ of gas each year, say, which would lead to a not unreasonable final mass of $\sim 3 \times 10^6 M_{\odot}$. The remaining $\sim 99\%$ of the gas in the nuclear region would make a nuclear star cluster or small pseudo-bulge, and some could be ejected through stellar and/or AGN feedback.

5.2. *Bars and AGN*

Fuel must be supplied to the accretion disk surrounding a central MBH in a galaxy in order for it to become active. We have shown that bar-driven gas inflow stalls at a nuclear ring when the galaxy hosts a massive central object that exceeds 1% of the disk mass. In our

idealized simulations, the nuclear ring makes a “water-tight” barrier that prevents the stalled gas from reaching the central engine. In reality, stellar feedback, magnetic fields, self-gravity, etc. may allow some slow leakage of gas from the ring to the nuclear region, but since the nuclear ring radius is many hundreds of times the scale of the accretion disk, only gas that has somehow shed over 99% of its angular momentum before reaching the accretion disk could fuel the MBH. These issues were reviewed by Jogee (2006).

Thus, except in very earliest stages of galaxy assembly before the massive central object has been created, our models predict little or no connection between the fueling of AGN and the presence of a bar in the disk; i.e. whatever causes AGN activity in galaxies should be largely unaffected by whether the galaxy hosts a bar. Furthermore, any possible relation between a bar and a MBH is likely to be erased by the possible self-destruction of the first bar and the formation of a new bar.

This prediction seems consistent with the findings of many observational studies that have examined the possible connection between large-scale bars and feeding of MBHs. Some authors have concluded that AGN activity is mildly enhanced in barred galaxies (e.g. Hao et al. 2009; Oh et al. 2012; Alonso et al. 2013; Galloway et al. 2015) but others have not (e.g. Kormendy & Ho 2013; Cheung et al. 2015). An additional study by Cisternas et al. (2015) used *Chandra* X-ray data to identify AGN and HST imaging to examine the morphology of galaxies out to $z \sim 0.84$ and also concluded that the presence of a bar had no influence on the strength of AGN activity. This body of work therefore suggests that, while a tendency for bars to cause a mild increase in AGN activity is not fully excluded, it is clearly not a strong effect.

Many of these papers examined low redshift ($z \lesssim 0.05$) samples of galaxies. Even the studies by Cheung et al. (2015) and Cisternas et al. (2015) out to $z \gtrsim 1$, used observations at an epoch that is long after our predicted early connection between bars and the creation of a MBH has been erased. An observational study at much higher redshift to test for a possible connection between the morphology of forming disks (see Erwin 2017, for a discussion of the detectability of bars) and AGN activity seems well beyond what is technically feasible today, and may even be beyond the reach of the James Webb Space Telescope.

In other theoretical work, Shlosman et al. (1989) proposed that nuclear gaseous rings could become dynamically decoupled from the bar that formed them, enabling a cascade of bar instability events that could drive gas closer and closer to the MBH, a picture that was refined by Hopkins & Quataert (2010) using multiscale SPH simulations. It seems hard to reconcile this predicted behavior with the weak, or non-existent, correlation between bars and AGN.

5.3. *Bar formation*

We assume that a bar forms quickly as the rotationally supported disk is being assembled, which is likely since disks are chronically unstable. Modern simulations (Athanasoula 2002; Saha & Naab 2013; Polyachenko et al. 2016) have shown that bars form far more readily in live halos than in rigid, and that bar for-

mation seems inevitable in rotationally supported disks of even quite low mass (Berrier & Sellwood 2016). These models also find that bars can form in halos with central density cusps, as happened in the model we employ here, and a harmonic core is therefore not required for bar formation. The only requirement to seed a MBH in the SM99 model is that the initial mass distribution of the disk plus halo should not include a massive central object that would cause the gas flow to stall at a radius of a few hundred parsec.

Observations of forming galaxies at $z \gtrsim 2$ reveal that they generally have a turbulent, irregular clumpy appearance (Elmegreen et al. 2007). However, they do seem to have significant rotation (Shapiro et al. 2008) and bar formation is hard to prevent even if the underlying mass distribution were as clumpy as the light (e.g. Du et al. 2015) which seems unlikely as the bright spots are believed to be areas of intense star formation.

5.4. Relation to the merger model of BH growth

SM99 proposed that a moderate mass MBH should be formed as the disk is being assembled and forms its first bar. The activity is self-limiting because the build-up of a central concentration causes the gas inflow to stall at a circum-nuclear ring, thereby starving the central engine of further fuel. These precursor MBHs are required to power quasar activity during subsequent mergers.

Furthermore, as reviewed in the introduction, the MBHs formed by the mechanism proposed by SM99 are required as modest central engines of Seyfert activity in galaxies lacking a significant classical bulge component. The absence of a substantial classical bulge is generally believed to indicate that the host galaxy has not experienced significant mergers as it was being assembled, as was stressed by Kormendy et al. (2010).

5.5. Limitations

Our simulations carefully compute the 2D flow of an ideal, isothermal gas, in a fixed-potential. But we neglect many complicating physical processes that might affect the gas flow and the ultimate fate of the gas accumulated in the galactic center.

We justify this approach because the sole science question we wished to address was how the mass of the accumulated gas in the center affects the subsequent flow pattern. The inflow happens so efficiently and quickly that star formation, feedback, and other “gastrophysics” can scarcely have time to affect the outcome, as Fanali et al. (2015) argued. The main effect is that the mass of gas that accumulates in the center alters the subsequent flow; whether the gas inside a few hundred parsec goes on to form stars and/or an MBH will not change this result.

Other studies have shown that increasing the sound speed (Kim et al. 2012b), including magnetic fields (Kim & Stone 2012), gas self-gravity (Wada 2004), or star-formation and stellar feedback (Izumi et al. 2016) could enable a moderate inflow to MBHs, even after the nuclear ring has developed. But these processes will influence the flow on a time scale that is long compared with that on which the ring was created, and would have little affect on the initial rapid growth of the MBH or the establishment of the nuclear ring (or ILR). On the other hand, any stellar and AGN feedback will likely hasten

the clearance of gas around the MBH, and may further shorten the duration of AGN activity. Therefore we consider that inclusion of these sub-grid physical processes would not qualitatively change our findings.

6. SUMMARY

We have performed hydrodynamical simulations of gas flows in a realistic N -body barred galaxy model that lacks a classical bulge. We found two distinct flow patterns depending upon the presence of a sufficiently massive central object. Without a central object, gas could be driven by the bar down to the very center, while the flow stops at a few hundred parsecs away from the center when the central object of at least $\sim 1\%$ disk mass is included. We have shown that the ring forms near an inner resonance, where the higher orbital frequencies cause the gas response to be perpendicular to the bar major axis – the generalization of the ILR from linear theory. By including self-gravity of the gas, and mimicking the formation of stars in a simplified way, we also showed that a central object of this mass could be created by the gas inflow itself.

We argue that moderate mass MBHs could be created in forming disk galaxies due gas inflow driven by the first bar in the disk. The activity of these MBHs is self-limiting because the build-up of a massive central object stalls the inflow at a nuclear ring, thereby bringing about the end of rapid growth of the MBH. We estimated the mass of the MBH formed during such a process to be $\sim 10^6 \sim 10^7 M_\odot$, which is typical of the masses of MBHs required for Seyfert activity in nearby galaxies having pseudobulges, but little or no classical bulge. The bar might also be destroyed if the central object is massive enough. Gas flows in any bar formed subsequently will stall at a nuclear ring, due to the continued existence of the massive central object, preventing accretion onto the MBH and leaving at most a weak correlation between bars and AGN today.

We thank an anonymous referee for some very constructive criticism that helped us to strengthen the paper, and also Luis Ho for valuable comments. The research presented here was partially supported by the 973 Program of China under grant no. 2014CB845700, by the National Natural Science Foundation of China under grant nos.11333003, 11322326, and by a China-Chile joint grant from CASSACA. A China Scholarship Council award (CSC, No.201604910905) supported ZL during a six-month visit to Rutgers University. We also acknowledge support from NSF grant AST/12117937 to JAS and a *Newton Advanced Fellowship* awarded by the Royal Society and the Newton Fund to JS, and from the CAS/SAFEA International Partnership Program for Creative Research Teams. This work made use of the facilities of the Center for High Performance Computing at Shanghai Astronomical Observatory.

REFERENCES

- Alonso, M. S., Coldwell, G. & Lambas, D. G. 2013, *A&A*, **549**, A141
 Athanassoula, E. 1992, *MNRAS*, **259**, 345
 Athanassoula, E. 2002, *ApJ*, **569**, L83
 Baldassare, V. F., Reines, A. E., Gallo, E. & Greene, J. E. 2017, arXiv:170907884

- Barentine, J. C. & Kormendy, J. 2012, *ApJ*, **754**, 140
- Berrier, J. C. & Sellwood, J. A. 2016, *ApJ*, **831**, 65
- Binney, J., Gerhard, O. E., Stark, A. A., Bally, J. & Uchida, K. I. 1991, *MNRAS*, **252**, 210
- Binney, J. & Tremaine, S. 2008, *Galactic Dynamics: Second Edition* (Princeton, Princeton University Press)
- Bonoli, S., Mayer, L. & Callegari, S. 2014, *MNRAS*, **437**, 1576
- Bournaud, F. & Combes, F. 2002, *A&A*, **392**, 83
- Boyle, B. J., Fong, R., Shanks, T. & Peterson, B. A. 1987, *MNRAS*, **227**, 717
- Buta, R. 1995, *ApJS*, **96**, 39
- Buta, R. & Block, D. L. 2001, *ApJ*, **550**, 243
- Cheung, E., Trump, J. R., Athanassoula, E., *et al.* 2015, *MNRAS*, **447**, 506
- Cisternas, M., Sheth, K., Salvato, M., *et al.* 2015, *ApJ*, **802**, 137
- Combes, F. & Sanders, R. H. 1981, *A&A*, **96**, 164
- Comerón, S., Knapen, J. H., Beckman, J. E., *et al.* 2010, *MNRAS*, **402**, 2462
- Contopoulos, G. & Grosbøl, P. 1989, *A&A Rev.*, **1**, 261-289
- Contopoulos, G. & Papayannopoulos, Th. 1980, *A&A*, **92**, 33
- Davies, R. L., Groves, B., Kewley, L. J., *et al.* 2017, *MNRAS*, **470**, 4974
- Debattista, V. P. & Sellwood, J. A. 2000, *ApJ*, **543**, 704
- Di Matteo, T., Springel, V. & Hernquist, L. 2005, *Nature*, **433**, 604
- Du, M., Shen, J. & Debattista, V. P. 2015, *ApJ*, **804**, 139
- Dubois, Y., Devriendt, J., Slyz, A. & Teyssier, R. 2012, *MNRAS*, **420**, 2662
- Ebisuzaki, T., Makino, J., Tsuru, T. G., *et al.* 2001, *ApJ*, **562**, L19
- Elmegreen, D. M., Elmegreen, B. G., Ravindranath, S. & Coe, D. A. 2007, *ApJ*, **658**, 763
- Erwin, P. 2017, preprint
- Fanali, R., Dotti, M., Fiacconi, D. & Haardt, F. 2015, *MNRAS*, **454**, 3641
- Few, C. G., Dobbs, C., Pettitt, A. & Konstantin, L. 2016, *MNRAS*, **460**, 4382
- Fragkoudi, F., Athanassoula, E. & Bosma, A. 2016, *MNRAS*, **462**, L41
- Fux, R. 1997, *A&A*, **327**, 983
- Fux, R. 1999, *A&A*, **345**, 787
- Galloway, M. A., Willett, K. W., Fortson, L. F., *et al.* 2015, *MNRAS*, **448**, 3442
- Gardiner, T. A. & Stone, J. M. 2005, *J. Comp. Phys.*, **205**, 509
- Gerin, M., Combes, F. & Nakai, N. 1988, *A&A*, **203**, 44
- González-Martín, O., Masegosa, J., Márquez, I., Guainazzi, M. & Jiménez-Bailón, E. 2009, *A&A*, **506**, 1107
- Hachelt, M. G. & Rees, M. J. 1993, *MNRAS*, **263**, 168
- Hao, L., Jogee, S., Barazza, F. D., Marinova, I. & Shen, J. 2009, in *Astronomical Society of the Pacific Conference Series*, Vol. 419, *Galaxy Evolution: Emerging Insights and Future Challenges*, ed. S. Jogee, I. Marinova, L. Hao & G. A. Blanc, 402
- Hawarden, T. G., Mountain, C. M., Leggett, S. K. & Puxley, P. J. 1986, *MNRAS*, **221**, 41P
- Hernquist, L. 1990, *ApJ*, **356**, 359
- Hopkins, P. F., Hernquist, L., Martini, P., *et al.* 2005, *ApJ*, **625**, L71
- Hopkins, P. F., Lidz, A., Hernquist, L., *et al.* 2007a, *ApJ*, **662**, 110
- Hopkins, P. F. & Quataert, E. 2010, *MNRAS*, **407**, 1529
- Hopkins, P. F., Richards, G. T. & Hernquist, L. 2007b, *ApJ*, **654**, 731
- Izumi, T., Kawakatu, N. & Kohno, K. 2016, *ApJ*, **827**, 81
- Jogee, S. 2006, in *Lecture Notes in Physics*, Berlin Springer Verlag, Vol. 693, *Physics of Active Galactic Nuclei at all Scales*, ed. D. Alloin, 143
- Jogee, S., Scoville, N. & Kenney, J. D. P. 2005, *ApJ*, **630**, 837
- Keselman, J. A. & Nusser, A. 2012, *MNRAS*, **424**, 1232
- Kim, W.-T., Seo, W.-Y. & Kim, Y. 2012a, *ApJ*, **758**, 14
- Kim, W.-T., Seo, W.-Y., Stone, J. M., Yoon, D. & Teuben, P. J. 2012, *ApJ*, **747**, 60
- Kim, W.-T. & Stone, J. M. 2012, *ApJ*, **751**, 124
- Kormendy, J., Drory, N., Bender, R. & Cornell, M. E. 2010, *ApJ*, **723**, 54
- Kormendy, J. & Ho, L. C. 2013, *ARA&A*, **51**, 511
- Kormendy, J. & Kennicutt, R. C. 2004, *ARA&A*, **42**, 603
- Kormendy, J. & Richstone, D. 1995, *ARA&A*, **33**, 581
- Krolik, J. H. 1999, *Active galactic nuclei* (Princeton: Princeton University Press)
- Krumholz, M. R. 2015, in *Astrophysics and Space Science Library*, Vol. 412, *Very Massive Stars in the Local Universe*, ed. J. S. Vink, 43
- Latif, M. A. & Ferrara, A. 2016, *PASA*, **33**, e051
- Li, Z., Shen, J. & Kim, W.-T. 2015, *ApJ*, **806**, 150
- Lin, L., Li, C., He, Y., Xiao, T. & Wang, E. 2016, *ArXiv e-prints*
- Luo, Y., Nagamine, K. & Shlosman, I. 2016, *MNRAS*, **459**, 3217
- Madau, P. & Rees, M. J. 2001, *ApJ*, **551**, L27
- Martini, P. 2004, In "Coevolution of Black Holes and Galaxies". Ed. L. C. Ho (Cambridge, Cambridge University Press), 169
- Mazzuca, L. M., Knapen, J. H., Veilleux, S. & Regan, M. W. 2008, *ApJS*, **174**, 337
- Merloni, A. & Heinz, S. 2008, *MNRAS*, **388**, 1011
- Morokuma-Matsui, K. & Baba, J. 2015, *MNRAS*, **454**, 3792
- Norman, C. A., Sellwood, J. A. & Hasan, H. 1996, *ApJ*, **462**, 114
- Oh, S., Oh, K. & Yi, S. K. 2012, *ApJS*, **198**, 4
- Ostriker, J. P. & Peebles, P. J. E. 1973, *ApJ*, **186**, 467
- Polyachenko, E. V., Berczik, P. & Just, A. 2016, *MNRAS*, **462**, 3727
- Rodriguez-Fernandez, N. J. & Combes, F. 2008, *A&A*, **489**, 115
- Saha, K. & Naab, T. 2013, *MNRAS*, **434**, 1287
- Sakamoto, K., Okamura, S. K., Ishizuki, S. & Scoville, N. Z. 1999, *ApJ*, **525**, 691
- Sanders, R. H. & Huntley, J. M. 1976, *ApJ*, **209**, 53
- Scannapieco, C., Wadeuhl, M., Parry, O. H., *et al.* 2012, *MNRAS*, **423**, 1726
- Sellwood, J. A. 2014, arXiv:1406.6606 (on-line manual: <http://www.physics.rutgers.edu/~sellwood/manual.pdf>)
- Sellwood, J. A. & McGaugh, S. S. 2005, *ApJ*, **634**, 70
- Sellwood, J. A. & Moore, E. M. 1999, *ApJ*, **510**, 125
- Sellwood, J. A. & Wilkinson, A. 1993, *Rep. Prog. Phys.*, **56**, 173
- Shapiro, K. L., Genzel, R., Förster Schreiber, N. M., *et al.* 2008, *ApJ*, **682**, 231
- Shapiro, S. L. & Teukolsky, S. A. 1985, *ApJ*, **298**, 58
- Shen, J., Rich, R. M., Kormendy, J., *et al.* 2010, *ApJ*, **720**, L72
- Shen, J. & Sellwood, J. A. 2004, *ApJ*, **604**, 614
- Shlosman, I., Frank, J. & Begelman, M. C. 1989, *Nature*, **338**, 45
- Singal, J., George, J. & Gerber, A. 2016, *ApJ*, **831**, 60
- Smith, A., Bromm, V. & Loeb, A. 2017, *ArXiv e-prints*
- Somerville, R. S. & Davé, R. 2015, *ARA&A*, **53**, 51
- Sormani, M. C., Binney, J. & Magorrian, J. 2015, *MNRAS*, **449**, 2421
- Stone, J. M. & Gardiner, T. 2009, *New A*, **14**, 139
- Stone, J. M., Gardiner, T. A., Teuben, P., Hawley, J. F. & Simon, J. B. 2008, *ApJS*, **178**, 137
- Toomre, A. 1981, In "The Structure and Evolution of Normal Galaxies", eds. S. M. Fall & D. Lynden-Bell (Cambridge, Cambridge Univ. Press) p. 111
- Toomre, A. & Toomre, J. 1972, *ApJ*, **178**, 623
- Treister, E., Schawinski, K., Urry, C. M. & Simmons, B. D. 2012, *ApJ*, **758**, L39
- van Albada, T. S. & Sanders, R. H. 1982, *MNRAS*, **201**, 303
- Wada, K. 2004, In "Coevolution of Black Holes and Galaxies". Ed. L. C. Ho (Cambridge, Cambridge University Press) p. 186 (astro-ph/0308134)
- Wytke, J. S. B. & Loeb, A. 2003, *ApJ*, **595**, 614